# Development of Perez-Du Mortier Calibration Algorithm for Ground-Based Aerosol Optical Depth Measurement with Validation using SMARTS Model

Jedol Dayou, Jackson Hian Wui Chang, Rubena Yusoff, Ag. Sufiyan Abd. Hamid, Fauziah Sulaiman, Justin Sentian

***Abstract***—Aerosols are small particles suspended in air that have wide varying spatial and temporal distributions. The concentration of aerosol in total columnar atmosphere is normally measured using aerosol optical depth (AOD). In long-term monitoring stations, accurate AOD retrieval is often difficult due to the lack of frequent calibration. To overcome this problem, a near-sea-level Langley calibration algorithm is developed using the combination of clear-sky detection model and statistical filter. It attempts to produce a dataset that consists of only homogenous and stable atmospheric condition for the Langley calibration purposes. In this paper, a radiance-based validation method is performed to further investigate the feasibility and consistency of the proposed algorithm at different location, day, and time. The algorithm is validated using SMARTS model based n DNI value. The overall results confirmed that the proposed calibration algorithm feasible and consistent for measurements taken at different sites and weather conditions.

***Keywords***—Aerosol optical depth, direct normal irradiance, Langley calibration, radiance-based validation, SMARTS.

## I. INTRODUCTION

IN long-term AOD monitoring networks, frequent calibration of the ground-based spectrometers is necessary to maintain its accuracy and reliability retrieval. Generally, calibration of spectrometer for AOD measurement can be performed using two methods: standard laboratory lamp or Langley calibration. Previous studies had reported that the former method is typically have inconsistent uncertainty [1] and also prohibitive with necessary power supplies, fragile, and have a limited lifespan [2]. Instead of using a calibrated lamp, the latter method is a passive calibration method that uses solar disc as the light source. It uses the progress of sun's apparent motion that changes the observed path length through the atmosphere to compute an optical depth. In this way, multiple measurement of solar irradiance at distinct air mass is feasible by measuring the sun's irradiance as the sun moves across the sky for significant changes of air mass.

In most AOD monitoring stations, Langley calibration is often a preferable selection over the absolute method. For instance, AEROENT, one of the largest AOD monitoring networks which has over hundreds stations worldwide, uses Langley calibration to calibrate its monitoring instrument periodically. In common practice, the reference instruments are typically recalibrated on a basis of 2-3 months cycle in high altitude (3400m) condition at Mauna Loa Observatory (MLO), for clear and aerosol-stable atmosphere.

However, regular access to high altitude for frequent is not efficient in terms of accessibility and economical prospects. On the other hand, if it is performed over low altitudes or near-sea-level sites, it is often complicated by the possible temporal drifts in the atmospheric condition during the calibration period [3]. This condition is even more severe for tropical atmosphere where cloud loading and rainfall is abundant throughout the year. Therefore, most instruments are calibrated against a reference instrument with a MLO-derived extrapolated value [4] but these secondary calibrated instruments typically have larger uncertainties than the reference instrument uncertainty [5].

In view of this, it is hypostasized that if there is a method to accurately approximate the clear sky condition at high altitude over near-sea-level sites, Langley calibration could be made feasible even at low altitudes. As a direct consequent, this can be useful to maintain the accuracy of AOD retrieval particularly for long-terms monitoring stations. For this purpose, a near-sea-level Langley calibration algorithm that uses the combination of clear-sky detection (PDM) model and statistical filter is developed for AOD measurement in a parallel work which was acceptable to be published in reference [6]. Details of the calibration algorithm are discussed in Section II. In this paper, a radiance-based validation method is performed to further investigate the feasibility and consistency of the proposed calibration algorithm at different location, day, and time.

J. Dayou is an Associate Professor with the e-VIBS, School of Science and Technology, UMS, Jalan UMS, 88400 Kota Kinabalu, Sabah, Malaysia. (Phone: +6-088-320000; Fax: +6-088-435324; e-mail: jed@ums.edu.my).

J. H. W. Chang is a postgraduate student with the e-VIBS, School of Science and Technology, UMS, Jalan UMS, 88400 Kota Kinabalu, Malaysia.

J. Sentian and F. Sulaiman are senior lecturer in School of Science and Technology, UMS, Jalan UMS, 88400 Kota Kinabalu.

R. Yusoff and A. S. Abd. Hamid are lecturers in School of Science and Technology, UMS, Jalan UMS, 88400 Kota Kinabalu.

## II. METHOD

### A. PDM Calibration Algorithm

The PDM calibration algorithm is an objective algorithm that constrains the Langley extrapolation using the combination of clear-sky detection (PDM) model and statistical filter. By combining these two approaches as an ensemble algorithm, a data set that is close to the homogenous and stable atmospheric condition could be selected from a continuous time series of measurement within a number of sufficient observations. In this way, the possible temporal drifts experienced by the atmosphere during the observation period can be minimized and possibly eliminated if the turbidity of that particular day itself is very low.

In the first part of the algorithm, the clear-sky detection model is used to ascertain only cloudless and clear sky data is selected for the regression. They consist of two sky-classification models which are Perez model and Du-Mortier model. Both models are selected because they had been proven to be appropriate in classifying the sky type under various weather conditions [7], [8]. The Perez model is one of the most acknowledged precise models and it is often used for predicting the daylighting in building design [7]. In Perez's model classification, the sky is classified into three type namely clear sky, intermediate blue and cloudy of overcast. It uses the Perez's clearness index as an indicator to classify the sky type which can be computed using the relationship between the diffuse $I_{ed}$ and global $I_{eg}$ horizontal irradiance as shown by [7]:

$$\varepsilon = \frac{(I_{ed} + I_{dir}/I_{ed}) + 1.041\phi_H}{1 + 1.041\phi_H} \qquad (1)$$

where $I_{dir}$ is the direct irradiance and $\phi_H$ is the solar zenith angle in radian. The second model is Du Mortier model which classifies sky condition into five type using Nebulosity index (NI) as indicator of sky type. The indicator NI is computed by the relationship between diffuse irradiance $I_d$, global irradiance $I$, and cloud ratio CR [8]:

$$NI = \frac{1 - I_d/I}{1 - CR} \qquad (2)$$

where CR is given by:

$$CR = \frac{I_{d,cl}}{\left[I_{d,cl} + \exp(-4mAr)\sin\alpha\right]} \qquad (3)$$

$I_{d,cl}$ and Ar represents the clear sky illuminance and Rayleigh scattering coefficient, respectively, given by:-

$$I_{d,cl} = 0.0065 + (0.255 - 0.138\sin\alpha)\sin\alpha \qquad (4)$$

$$Ar = \{5.4729 + m[3.0312 + m\{-0.6329 + m(0.091 - 0.00512m)\}]\}^{-1} \qquad (5)$$

where $m$ is the optical air mass and $\alpha$ is the solar altitude. In the proposed algorithm, the Perez and Du Mortier Model are used together to form a combined sky classification as shown in Table I.

TABLE I
PEREZ AND DU MORTIER SKY CLASSIFICATION

| Value of Indices | | Sky Conditions |
|---|---|---|
| Nebulosity index, NI | Clearness index, $\epsilon$ | |
| $0.95 \leq NI \leq 1.00$ | $\epsilon \geq 4.50$ | Ideal clear sky |
| $0.70 \leq NI < 0.95$ | $1.23 < \epsilon < 4.50$ | Intermediate blue |
| $0.20 \leq NI < 0.70$ | $*\epsilon \leq 1.23$ | Intermediate mean / *Cloudy overcast |
| $0.05 \leq NI < 0.20$ | $*\epsilon \leq 1.23$ | Intermediate overcast/ *Cloudy overcast |
| $0.00 \leq NI < 0.05$ | $*\epsilon \leq 1.23$ | Overcast/ *Cloudy overcast |

In the second part of the algorithm, the statistical filter is used to filter the resulting regression for improved instrument's response. The statistical filter used in the proposed method adopted the similar approach suggested by [9]. The filter works in a way that a successful Langley plot should remain a minimum of one-third points with a standard deviation around the regression line of less than $2\sigma$. Implicitly, pixels $P_\lambda$ values with residual standard deviation greater than $\pm 2\sigma$ from the mean will be removed from the analysis. The function of the statistical filtration is to reduce the field-of-view effects associated to the uncertainties caused by the diffuser used to overfill the image of the sun from the radiometer to retrieve the direct solar beam. By doing this, possible outliers and instabilities due to the instrument responses can be possibly eliminated. In addition, this error estimator is a ratio of intensities, and hence is independent of both the evolution of air mass as well as the absolute calibration of the detector [9].

Basically, the PDM calibration algorithm constrains the Langley extrapolation based on repetitive regression algorithm using multiple permutated criteria (NI$_x$, $\varepsilon_x$) until the best linearity between natural logarithm of pixels and air mass is obtained. The advantage of using only clear-sky data defined by the proposed algorithm is that noise is reduced and a confident extrapolation to zero air mass by simple regression is feasible. Instead of using a single day for Langley plot, the proposed method collects several days of clear-sky Langley plots over a period of time. In this way, it produces a pool of extrapolated values so that a reliable mean can be computed. Since the proposed algorithm depends on the highest correlation plotted from the pool of screened data, it also increases the confidence that the mean extrapolated value is stable and free of any effects that promote changes in thin cirrus cloud and aerosol loading.

### B. Retrieval of AOD and Calibration Factor

By obtaining the mean extrapolated value from the Langley plot using least-square regression method, retrieval of total optical depth $\tau_{T,\lambda}$ is hence possible using the Beer-Lamber law of exponential as:

$$I_\lambda = l^2 I_{o,\lambda} \exp(-\sum \tau_{\lambda,i} m_i) \qquad (6)$$

where $I_\lambda$ is the direct normal irradiance at the ground (or near-sea-level) at wavelength $\lambda$, $l$ is the Earth-to-Sun distance in astronomical units (AU), $I_{o,\lambda}$ is the extraterrestrial irradiance at the top of atmosphere (TOA), $\tau_{\lambda,i}$ is the total optical depth of the $i$-th scatterer or absorber, and mi is the air mass of the $i$-th scatterer or absorber through the atmosphere.

Subsequently, the AOD $\tau_{a,i}$ is computed by subtracting the $\tau_\lambda$ from other relevant optical depth as:

$$\tau_{\lambda,i} = \tau_{R,i} + \tau_{o,i} + \tau_{a,i} \qquad (7)$$

where $\tau_{R,i}$ and $\tau_{O,I}$ are Rayleigh and Ozone optical depth, respectively, which can be estimated by:

$$\tau_{R,\lambda,i} = k_{Ray}(\lambda) \frac{p}{p_o} \exp(-\frac{H}{7998.9}) \qquad (8)$$

$$\tau_{o,\lambda,i} = Z \times k_{oz}(\lambda) \times 2.69e16 \, mol/cm^2 \qquad (9)$$

In (8), (9), $k_{Ray(\lambda)}$ and $k_{oz(\lambda)}$ are the Rayleigh scattering coefficient and ozone absorption cross section, respectively, $p$ is the site's atmospheric pressure, $p_o$ is the mean atmospheric pressure at sea-level, $H$ is the altitude from sea-level in meter, and $Z$ is ozone concentration in DU.

Also employing the mean extrapolated value obtained from the PDM calibration algorithm, determination of calibration factor, $k$ is feasible by dividing it with the extraterrestrial constant at top-of-atmosphere (TOA) in W/m$^2$/nm. Then, multiplication of the measured signal with this factor converts the pixels (measured using the ground-based spectrometer) into DNI as [2]

$$I_\lambda = P_\lambda k = \frac{P_\lambda \int P_{o,\lambda(avg)} F_\lambda d\lambda}{I_{o,\lambda} \int F_\lambda d\lambda} \qquad (10)$$

where $P_\lambda$ is the measured signal in pixel, $P_{o,\lambda}$ is the extrapolated value from Langley plot, and $I_{o,\lambda}$ is the extraterrestrial constant at TOA in W/m$^2$/nm.

### C. Radiance-Based Validation

In order to investigate the feasibility of the proposed calibration algorithm, the retrieved AOD is inserted into a radiative transfer model, SMARTS to simulate reference direct normal irradiance (DNI) at distinct air mass and different weather condition. In this way, direct comparison with the corresponding predicted DNI is hence feasible at each observation. By taking advantage the sensitivity of AOD on the changes in solar irradiance under clear-sky condition [10], this radiance-based validation method indirectly reverse-

validates the retrieved AOD as well as the calibration factor. Finally, the predicted DNI is then directly compared with the simulated value to allow radiance-based validation as shown in Fig. 1.
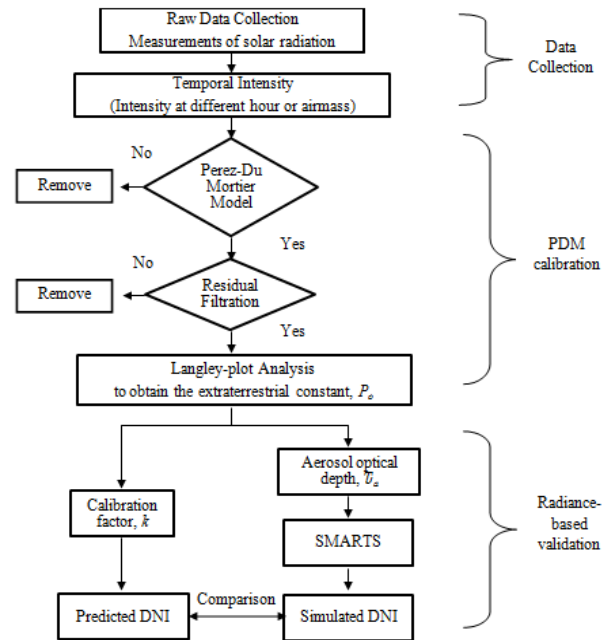


Fig. 1 Flowchart of the radiance-based validation methodology scheme

### III. DATA

In the current work, a portable ground-based spectrometer ASEQ LR-1 was used to collect solar spectral data over two study areas with different location, day, and time. In this way, the obtained results are useful to investigate the feasibility and consistency of the proposed algorithm in spatial and temporal aspects. Details of both locations are depicted in Table II. These sites are suitable for the solar spectrum observation because the observed spectrum is obstruct-free from irrelevant objects such as trees or artificial buildings.

TABLE II
DESCRIPTION OF THE STUDY AREA AND ITS OBSERVATION SCOPE

| Site | Menara Tun Mustapha | SST, UMS* |
|---|---|---|
| Site altitude (m) | 7.844 | 20.398 |
| Ground level (m) | 0.900 | 0.934 |
| Longitude | 6.02°N, 116.01°E | 6.04°N, 116.03°E |
| Observation period | 1$^{st}$ April – 31$^{st}$ May 2012 | 1$^{st}$ July – 31$^{st}$ August 2012 |
| Measurement time | 0630 – 0830 | 1030 – 1430 |
| Air mass | 2.0 – 6.0 | 1.0 – 1.2 |

* School of Science & Technology, Universiti Malaysia Sabah

To contain the spectral effect of reduced photodiode sensitivity at certain wavelengths, only 500nm was selected for the analysis. This particular wavelength is selected because it has good reproducibility and stabilities [11]. Besides, it also falls within the near-visible range where most spectrometers have optimum relative response and less affected by other

atmospheric constituents other than Rayleigh and ozone contribution.

In order to validate the irradiance values predicted by the proposed calibration algorithm in (10), simulated irradiance value obtained from radiative transfer model SMARTS version 2.9.5 is adopted as the true value. This model is documented in FSEC Report PF-270-95 and its accuracy is discussed in elsewhere [12], [13]. The simulation runs is repeated for each observation with distinct air mass and AOD values so that direct comparison between predicted and simulated irradiance values is feasible.

Other input parameters that required in SMARTS algorithm are the atmospheric pressure, air temperature, relative humidity, zenith angle, azimuth, etc., which are all measured quantities provided by local meteorological department. Table III presents the input parameters inserted into SMARTS model for the irradiance simulation. Parameters such as $CO_2$ and $O_3$ concentration that unable to obtain from local meteorological were averaged according to the spatial and temporal valuation of the study area using satellite observations provided by NOAA and NASA.

TABLE III
INPUT PARAMETERS FOR THE IRRADIANCE SIMULATION USING SMARTS

| Input parameters | Menara Tun Mustapha | SST, UMS |
|---|---|---|
| Altitude (m) | 7.844 | 20.398 |
| Latitude | 6.02°N, 116.01°E | 6.04°N, 116.03°E |
| Height above ground (m) | 0.900 | 0.934 |
| Reference atmosphere | Tropical (summer/spring season) | |
| Relative humidity | 75% | |
| Instantaneous temperature | 299.5K | |
| Regional albedo | 0.31 | |
| Aerosol Model | Shuttle & Fenn Urban (SFU) Model | |
| Solar constant | 1366.1 W/m$^2$/nm | |
| $CO_2$ mixing ratio (ppmv) | 394.01 | 393.01 |
| $O_3$ concentration (atm-cm) | 0.2611 | 0.2641 |

IV. RESULTS AND DISCUSSION

In this paper, a 2-month period of measurement had been collected for each study area. Within the observation period, a total of 730 and 535 raw data were collected over Menara Tun Mustapha and SST, UMS, respectively. However, not all data can be used due to cloud contamination. After the clear-sky filtration, the raw data was reduced to 205 and 241 useful data for each study area. Using the mean extrapolated value obtained from the proposed algorithm, the total optical depth $\tau_T$ was determined using (6). By having $\tau_T$ for each observation, corresponding optical depths $\tau_R$, $\tau_O$, and $\tau_a$ are then retrievable using (7)-(9). Subsequently, the retrieved $\tau_a$ was inserted into SMARTS model for solar insolation prediction, which will be adopted as true value for the point-by-point validation purposes.

Then, each measured signal collected from the observation is converted into direct normal irradiance (DNI) using (10). These values are hereinafter termed as predicted DNI for easy discussion whereas the simulated irradiance values obtained from SMARTS model are denoted as reference DNI to avoid confusion. Due to the large amount of data available, only selected day was presented the DNI data for each study area in Tables IV (Menara Tun Mustapha) and V (SST, UMS).

From Tables IV and V, it is obvious that the predicted DNI closely matches the reference values with small margin of error. To visualize the distribution of the predicted and reference DNI for the two study areas, histogram of the occurrence for both values are plotted in Fig. 2. In comparison with both values, the distribution is roughly similar where the pattern exhibits a positive-skewed Gaussian distribution. It should be noted that no specific reason is inherit in this pattern as the DNIs obtained over the second study area are relatively higher than the first study area due to lower air mass. In both cases, highest frequency of the measurement is observed in the same bin.

TABLE IV
TRUNCATED DATA FOR OPTICAL DEPTHS AND DNI IN W/M$^2$/NM AT WAVELENGTH 500NM OVER STUDY AREA MENARA TUN MUSTAPHA, KOTA KINABALU IN APR-MAY 2012 (TOTAL DATA, N=205)

| Time | Optical depth | | | | DNI, W/m$^2$/nm | |
|---|---|---|---|---|---|---|
| | $\tau_T$ | $\tau_R$ | $\tau_O$ | $\tau_a$ | Pd | Rf |
| 0652 | 0.202 | 0.143 | 0.008 | 0.051 | 0.573 | 0.561 |
| 0655 | 0.197 | 0.143 | 0.008 | 0.046 | 0.637 | 0.628 |
| 0658 | 0.205 | 0.143 | 0.008 | 0.054 | 0.658 | 0.643 |
| 0701 | 0.204 | 0.143 | 0.008 | 0.052 | 0.706 | 0.694 |
| 0707 | 0.202 | 0.143 | 0.008 | 0.051 | 0.790 | 0.784 |
| 0710 | 0.202 | 0.143 | 0.008 | 0.051 | 0.827 | 0.826 |
| 0713 | 0.198 | 0.143 | 0.008 | 0.047 | 0.877 | 0.877 |
| 0716 | 0.196 | 0.143 | 0.008 | 0.045 | 0.915 | 0.913 |
| 0719 | 0.197 | 0.143 | 0.008 | 0.045 | 0.944 | 0.936 |
| 0725 | 0.191 | 0.143 | 0.008 | 0.040 | 1.017 | 1.009 |
| 0728 | 0.196 | 0.143 | 0.008 | 0.044 | 1.028 | 1.026 |
| 0731 | 0.196 | 0.143 | 0.008 | 0.045 | 1.051 | 1.052 |
| 0734 | 0.200 | 0.143 | 0.008 | 0.048 | 1.063 | 1.066 |
| 0737 | 0.199 | 0.143 | 0.008 | 0.048 | 1.087 | 1.091 |
| 0740 | 0.210 | 0.143 | 0.008 | 0.059 | 1.073 | 1.077 |
| 0746 | 0.216 | 0.143 | 0.008 | 0.065 | 1.096 | 1.094 |
| 0749 | 0.219 | 0.143 | 0.008 | 0.068 | 1.106 | 1.098 |
| 0755 | 0.222 | 0.143 | 0.008 | 0.071 | 1.130 | 1.133 |
| … | … | … | … | … | … | … |

Pd: Predicted, Rf: Reference derived using SMARTS model

TABLE V
TRUNCATED DATA FOR OPTICAL DEPTHS AND DNI IN W/M²/NM AT
WAVELENGTH 500NM OVER STUDY AREA SST, UNIVERSITI MALAYSIA
SABAH IN JUL-AUG 2012 (TOTAL DATA, N=241)

| Time | Optical depth | | | | DNI, W/m²/nm | |
|------|------|------|------|------|------|------|
| | $\tau_T$ | $\tau_R$ | $\tau_O$ | $\tau_a$ | Pd | Rf |
| 1032 | 0.550 | 0.143 | 0.008 | 0.399 | 1.009 | 1.009 |
| 1126 | 0.504 | 0.143 | 0.008 | 0.353 | 1.116 | 1.110 |
| 1128 | 0.497 | 0.143 | 0.008 | 0.346 | 1.125 | 1.125 |
| 1130 | 0.497 | 0.143 | 0.008 | 0.346 | 1.127 | 1.127 |
| 1132 | 0.501 | 0.143 | 0.008 | 0.350 | 1.123 | 1.123 |
| 1134 | 0.486 | 0.143 | 0.008 | 0.335 | 1.142 | 1.142 |
| 1226 | 0.556 | 0.143 | 0.008 | 0.405 | 1.072 | 1.072 |
| 1228 | 0.571 | 0.143 | 0.008 | 0.420 | 1.055 | 1.055 |
| 1230 | 0.574 | 0.143 | 0.008 | 0.423 | 1.052 | 1.052 |
| 1232 | 0.557 | 0.143 | 0.008 | 0.406 | 1.070 | 1.070 |
| 1234 | 0.569 | 0.143 | 0.008 | 0.418 | 1.056 | 1.056 |
| 1330 | 0.590 | 0.143 | 0.008 | 0.439 | 1.005 | 1.005 |
| 1332 | 0.580 | 0.143 | 0.008 | 0.429 | 1.014 | 1.014 |
| 1334 | 0.583 | 0.143 | 0.008 | 0.432 | 1.010 | 1.010 |
| … | … | … | … | … | … | … |

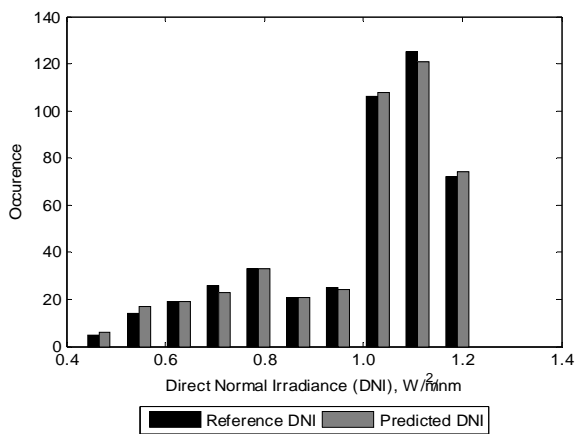Pd: Predicted, Rf: Reference derived using SMARTS model



Fig. 2 Frequency distribution of predicted and reference DNI at
wavelength 500nm

To study the relationship between both values, the correlation analysis is performed by plotting the reference DNI against the predicted value, where a simple regression is feasible to determine the corresponding correlation.

Fig. 3 shows the high linearity between both values at wavelength 500nm. The linear regression obtained in the plot when extrapolated to absolute zero intercepts almost at origin. The high coefficient of determination, $R^2 > 0.98$ verifies that the predicted value is highly correlated to the reference values where both increment and decrement observed in the measured signal are sensitive to the DNI.
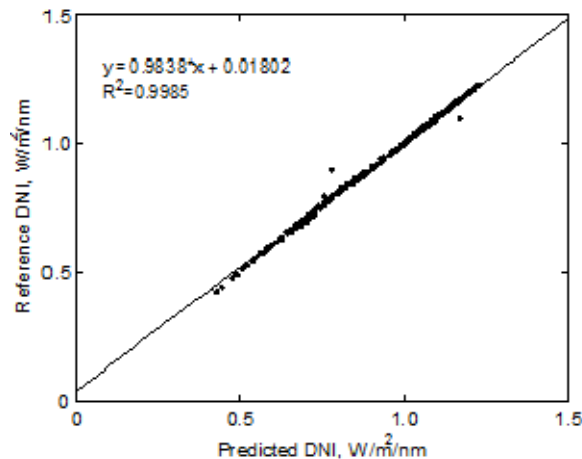


Fig.3 Correlation analysis plot between predicted and reference DNI
at 500nm

Though nearly similar distribution pattern and highly correlation are observed for both cases, slight differences can still be detected. The magnitude of these differences can be further assessed by examining their statistical properties derived from both cases. These values are tabulated in Table VI for easy comparison. From the table, it is clear that on average the predicted DNI agrees well to the reference value with small susceptible error of Normalize Mean Square Error (NMSE) less than 0.02% (RMSE ~0.01).

TABLE VI
STATISTICAL COMPARISON BETWEEN PREDICTED AND REFERENCE DNI AT
WAVELENGTH 500NM OVER TWO STUDY AREAS

| Statistical properties | Direct Normal Irradiance (DNI), W/m²/nm | | | |
|------|------|------|------|------|
| | Menara Tun Mustapha (n=205) | | SST, UMS (n=241) | |
| | Pd | Rf | Pd | Rf |
| min | 0.43 | 0.43 | 0.94 | 0.94 |
| max | 1.16 | 1.17 | 1.23 | 1.23 |
| mean | 0.85 | 0.85 | 1.10 | 1.10 |
| median | 0.84 | 0.85 | 1.11 | 1.11 |
| mode | 1.05 | 0.43 | 1.17 | 0.94 |
| std | 0.19 | 0.19 | 0.06 | 0.06 |
| range | 0.74 | 0.74 | 0.29 | 0.29 |
| RMSE | 0.01 | | 0.005 | |
| NMSE (%) | 0.02 | | 0.02 | |

## V. CONCLUSION

In this paper, a radiance-based validation method had been performed on a 4-month period of measurement over two study areas with different location, day, and time to investigate the feasibility and consistency of the PDM calibration algorithm. The radiance-based validation method validates the proposed algorithm by inverting the derived AODs into SMARTS model for DNI simulation. In this way, the comparison between the predicted and simulated DNI is hence feasible at each observation to allow point-by-point validation. Within the collected data, it is not possible to observe significant discrepancy between both values. In overall statistical comparison, the algorithm provides high linearity

between predicted and reference DNI value derived from SMARTS model with low susceptible error NMSE of less than 0.02%. This confirms that the proposed calibration algorithm is feasible and consistent even for measurement taken at different site and weather condition.

### REFERENCES

[1] P. W. Kiedron, J. J. Michalsky, J. L. Berndt, and L. C. Harrison, "Comparison of spectral irradiance standards used to calibrate shortwave radiometers and spectroradiometers," *Applied Optics*, vol. 38, no. 2, pp. 2432–2439, 1999.

[2] J. Slusser, J. Gibson, B. David, D. Kolinski, P. Disterhoft, K. Lantz, and A. Beaubien, "Langley method for calibrating UV filter radiometer," *Journal of Geophysical Research*, vol. 105, no. D4, pp. 4841–49, 2000.

[3] G. E. Shaw, "Sunphotometry," *Bulletin of the American Meteorological Society*, vol. 64, no. 1, pp. 4–10, 1983.

[4] T. M. Saeed and H. Al-Dashti, "Optical and physical characterization of 'Iraqi freedom' dust storm, a case study," *Theoretical and Applied Climatology*, vol. 104, no. 1–2, pp. 123–137, Sep. 2010.

[5] B. N. Holben, T. F. Eck, I. Slutske, D. Tanre, J. P. Buis, A. Setzer, E. Vermote, J. A. Reagan, Y. J. Kaufman, T. Nakajima, F. Lavenu, I. Jankowiak, and A. Smirnov, "AERONET-A Federated Instrument Network and Data Archive for Aerosol Characterization," *Remote Sensing of Environment*, vol. 66, pp. 1–16, 1998.

[6] J. H. W. Chang, J. Dayou, and J. Sentian, "Development of near-sea-level calibration algorithm for aerosol optical depth measurement using ground-based spectrometer," *To appear in Aerosol and Air Quality Research*, 2013.

[7] H. Djamila, C. C. Ming, and S. Kumaresan, "Estimation of exterior vertical daylight for the humid tropic of Kota Kinabalu city in East Malaysia," *Renewable Energy*, vol. 36, no. 1, pp. 9–15, Jan. 2011.

[8] A. Zain-Ahmed, K. Sopian, Z. Z. Abidin, and M. Y. H. Othman, "The availability of daylight from tropical skies — a case study of Malaysia," *Renewable Energy*, vol. 25, pp. 21–30, 2002.

[9] L. Harrison and J. Michalsky, "Objective algorithms for the retrieval of optical depths from ground-based measurements." *Applied optics*, vol. 33, no. 22, pp. 5126–32, Aug. 1994.

[10] J. H. W. Chang, J. Dayou, and J. Sentian, "Diurnal Evolution of Solar Radiation in UV , PAR and NIR Bands in High Air Masses," *Nature, Environment and Pollution Technology*, vol. 12, no. 1, pp. 1–6, 2013.

[11] J. H. W. Chang, J. Dayou, and J. Sentian, "Investigation of Short Time Scale Variation of Solar Radiation Spectrum in UV , PAR , and NIR Bands due to Atmospheric Aerosol and Water Vapor," *World Academy of Science, Engineering and Technology*, vol. 73, pp. 1112–1117, 2013.

[12] C. A. Gueymard, "Prediction and validation of cloudless shortwave solar spectra incident on horizontal, tilted, or tracking surfaces," *Solar Energy*, vol. 82, pp. 260–271, 2008.

[13] D. G. Kaskaoutis and H. D. Kambezidis, "The role of aerosol models of the SMARTS code in predicting the spectral direct-beam irradiance in an urban area," *Renewable Energy*, vol. 33, pp. 1532–1543, 2008.